# Supporting Information

## Bi-Cu bimetallenes array/carbonic anhydrase biohybrid for efficient and selective $CO_2$ electroreduction at low concentration†

Minli Shu,[a] Xuefang Zhu,[a] Zhe Wang,[a] Xue Xiao,[b*] Shuni Li,[a] Yu Chen[b*] and Yucheng Jiang[a*]

[a] Key Laboratory of Macromolecular Science of Shaanxi Province, School of Chemistry and Chemical Engineering, Shaanxi Normal University, Xi'an 710119, PR China.

[b] School of Materials Science and Engineering, Shaanxi Normal University, Xi'an 710119, PR China.

Corresponding authors:

E-mail: tiffanyxx110@gmail.com (X. Xiao); ndchenyu@gmail.com (Y. Chen); jyc@snnu.edu.cn (Y. Jiang)

## Experimental section

### 1. Electrochemical measurements

Electrochemical experiments were performed using a CHI 760E workstation with an H-type electrolytic cell separated with Nafion 117 membrane operating at room temperature. A silver/silver chloride (Ag/AgCl) was used as the reference electrode, the carbon rod electrode was used as the opposite electrode, and the modified electrode was used as the working electrode. The phosphate buffer solution (PBS, 0.1 M, 80 mL, pH = 6.5) was evenly divided into cathode and anode compartments. Carbon dioxide is injected into the cathode for electrochemical reduction if it is saturated. All potentials correspond to RHE, where RHE = $E_{Ag/AgCl}$ + 0.197 V + 0.0591pH.[1]

### 2. Ultraviolet detection

The loading amounts of CA were measured by ultraviolet-visible spectrophotometer (UV-vis, Cary60). The protein content was measured by the Coomassie bright blue method. The content of CA before and after loading was compared and the enzyme loading was calculated.[2]

### 3. Product detection

Gaseous products including $H_2$ was measured by gas chromatography on a zhejiangfili GC9700II equipped with two FID hydrogen flame ionization detectors and one TCD thermal conductivity cell detecto rand using Ar as a carrier gas. The liquid phase products were detected by nuclear magnetic resonance (NMR; 400 MHz, JNM-ECZ400R/S1, JEOL) using 500 μL of reaction electrolyte and 100 μL of $D_2O$ as solvent and 50 μL of DMSO-$d_6$ as internal standard.[3]

### 4. Computational methods

The gas product is calculated by the following formula:

$$FE_{gas} = \frac{Z \times F \times V(mL\ min^{-1}) \times v(vol\ \%) \times P}{R \times T \times I_{total} \times 60(s\ min^{-1})} \quad (1)$$

where $F$ is the Faraday constant (96485 C·mol$^{-1}$), $Z$ is the electron transfer number, $V$ is the gas flow rate obtained using a flow meter (5 mL·min$^{-1}$), $P$ is one atmosphere ($1.013 \times 10^5$ Pa), $R$ is the universal gas constant (8.314 J·mol$^{-1}$·K$^{-1}$), $I$ is the total steady-state cell current, and $T$ is the room temperature (298.15 K).[4]

The liquid phase product is calculated by the following formula:

$$FE_{HCOOH} = \frac{Z \times F \times n_{products}}{Q} \times 100\% \quad (2)$$

where $Q$ denotes the total charge ($C$) and *products* denote the moles of the obtained formic acid calculated by $^{1}$H-NMR.

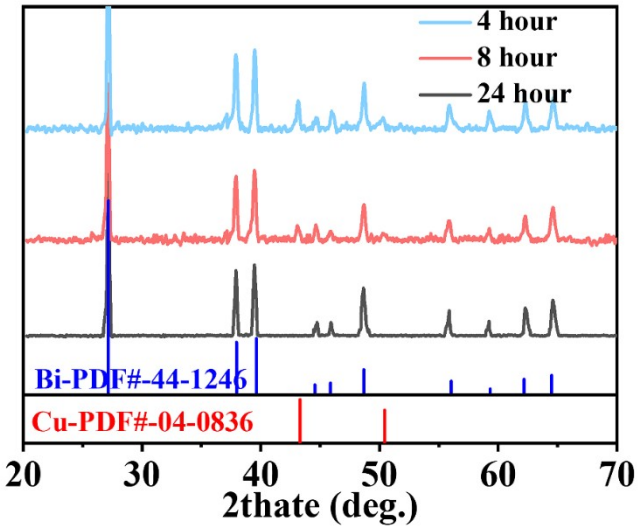


**Fig. S1.** XRD patterns of Bi-Cu BMLs at different growth times.

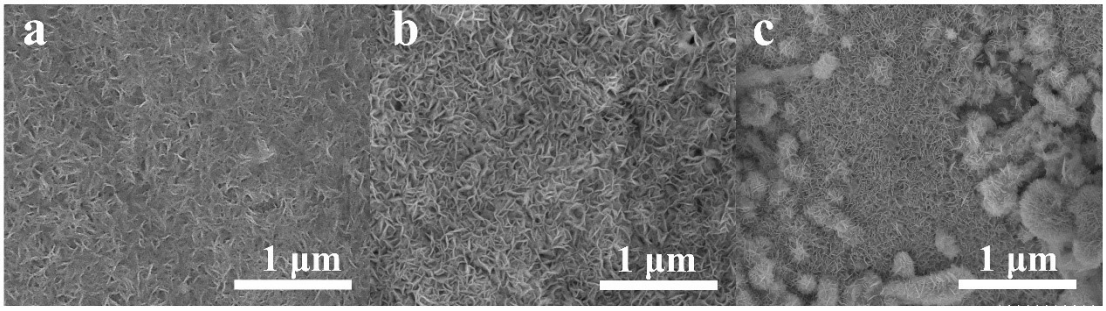


**Fig. S2.** SEM images of Bi-Cu BMLs with different growth times (a) 3 h, (b) 4 h, and (c) 5 h.

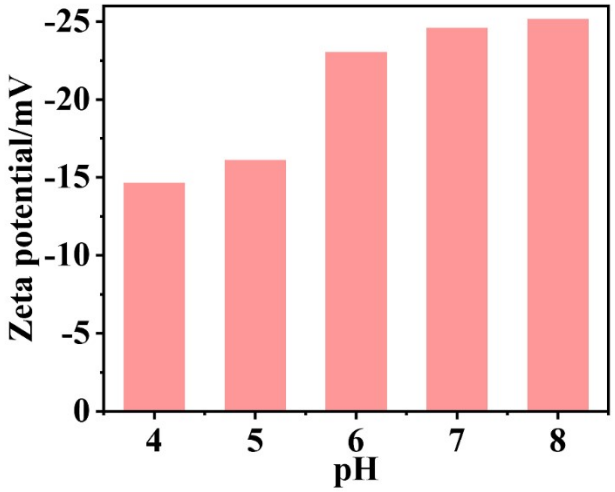


**Fig. S3.** Zeta potentials of Bi-Cu BMLs in PBS with different pH.

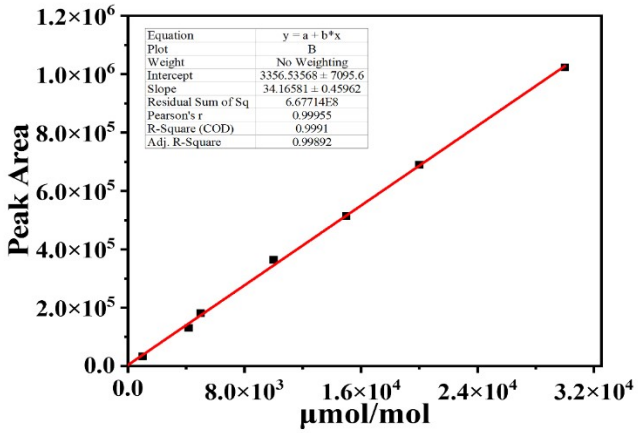


**Fig. S4.** Standard curves of different concentrations of CA versus UV-vis absorption.

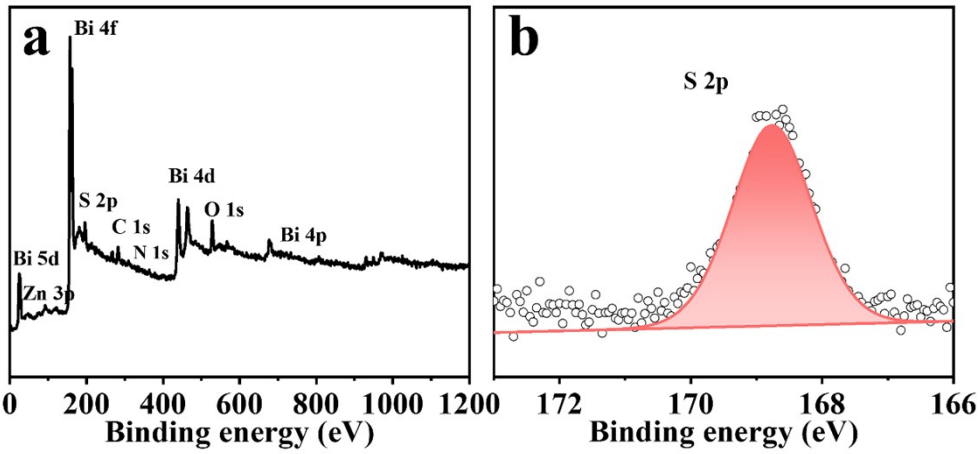


**Fig. S5.** (a) XPS full spectrum of CA/Bi-Cu BMLs biohybrid and (b) S 2p XPS spectrum of CA/Bi-Cu BMLs biohybrid.

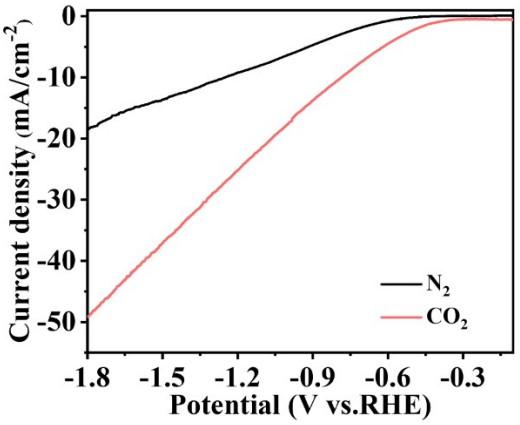


**Fig. S6.** LSV curves of CA/Bi-Cu BMLs biohybrids in in 0.1 M PBS with $CO_2$ and $N_2$ atmospheres 10 $mV \cdot s^{-1}$.

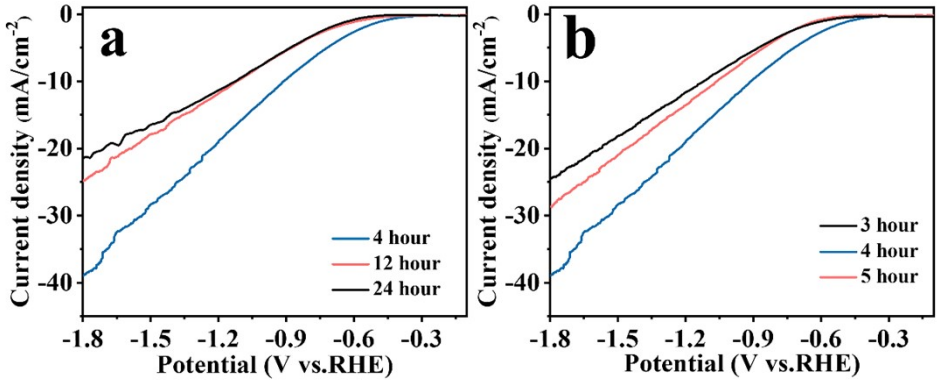


**Fig. S7.** LSV curves of Bi-Cu BMLs under different growth times in 0.1 M PBS at 10 $mV \cdot s^{-1}$.

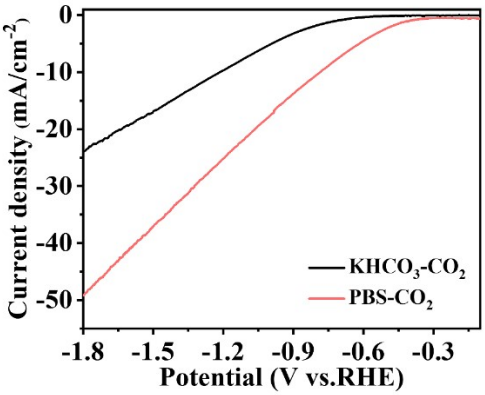


**Fig. S8.** LSV curves of CA/Bi-Cu BMLs biohybrid in 0.1 M PBS or 0.1 M $KHCO_3$ at pH 6.5 at 10 $mV \cdot s^{-1}$.

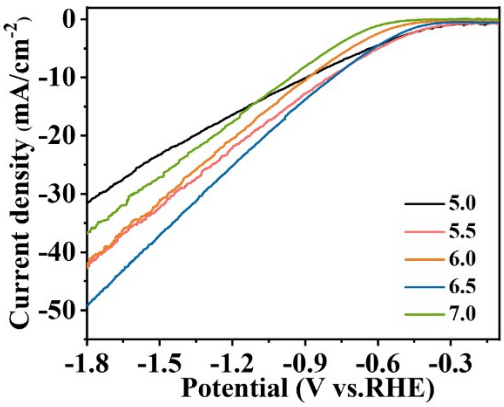


**Fig. S9.** LSV curves of CA/Bi-Cu BMLs biohybrid in PBS solutions at different pH at 10 $mV \cdot s^{-1}$.

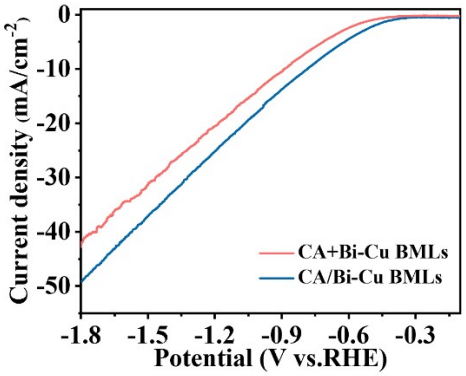


**Fig. S10** LSV curves of Bi-Cu BMLs with 0.08 mg CA in PBS and CA/Bi-Cu BMLs biohybrid at pH 6.5 at 10 $mV \cdot s^{-1}$.

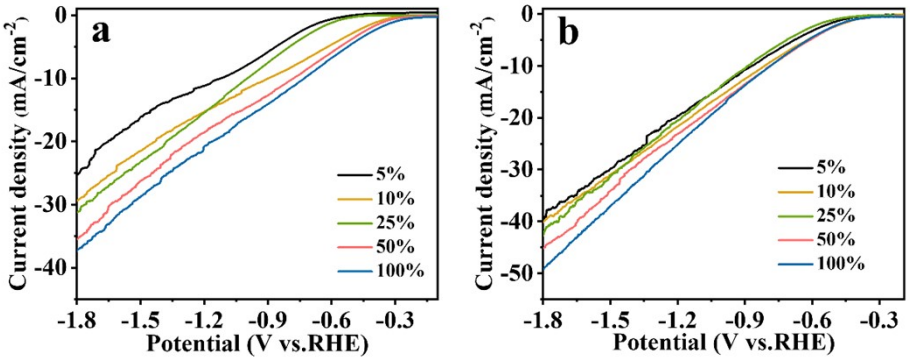


**Fig. S11.** LSV curves of (a) CA/Bi-Cu BMLs biohybrid and (b) Bi-Cu BMLs in 0.1 M PBS with different $CO_2$ concentrations at 10 $mV \cdot s^{-1}$.

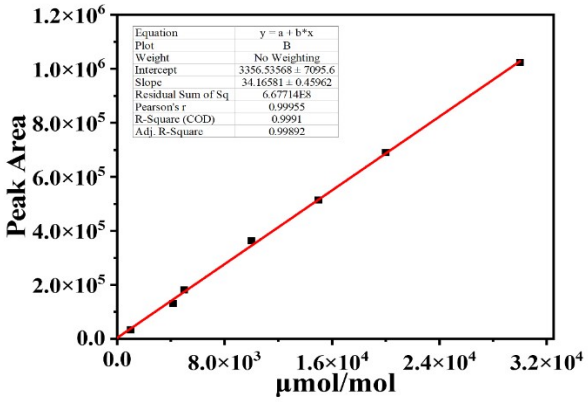


**Fig. S12.** Standard curve of $H_2$.

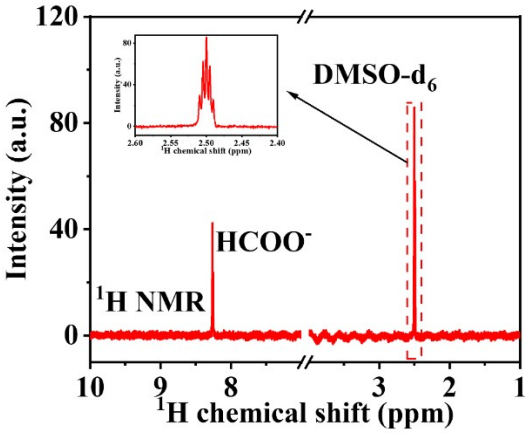


**Fig. S13** The $^1$H NMR of the product of $CO_2$RR by CA/Bi-Cu BMLs biohybrid using DMSO-$d_6$ as an internal standard.

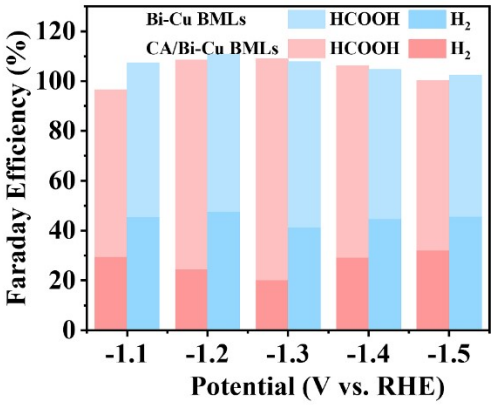


**Fig. S14.** Faraday efficiency of $CO_2$RR by CA/Bi-Cu BMLs biohybrid and Bi-Cu BMLs at different potentials.

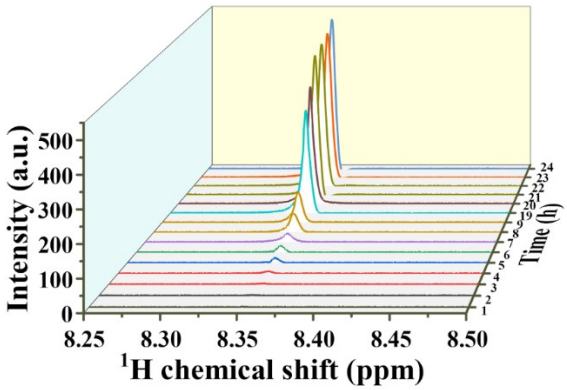


**Fig. S15** $^1$H NMR plots of formic acid at -1.3 V vs. RHE potential for different testing times.

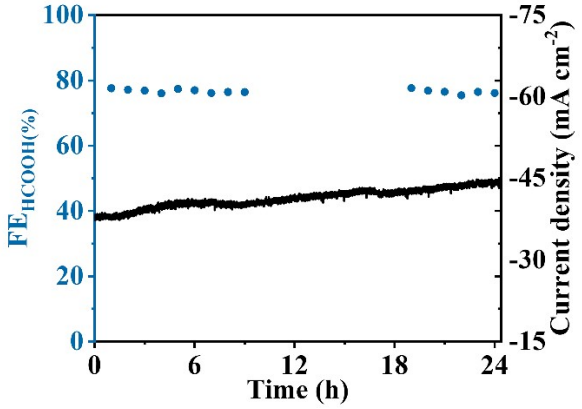


**Fig. S16** Catalytic stability test of CA/Bi-Cu BMLs biohybrid at 5% $CO_2$ concentration and $FE_{HCOOH}$ of $CO_2$RR at CA/Bi-Cu BMLs at -1.3 V vs. RHE for 24 h.

**References**


1 S. Jia, Q. Zhu, H. Wu, M. Chu, S. Han, R. Feng, J. Tu, J. Zhai and B. Han, *Chinese J. Catal.*, 2020, **41**, 1091–1098.

2 P. Koutnik, E. G. Shcherbakova, S. Gozem, M. G. Caglayan, T. Minami and P. Anzenbacher, *Chem*, 2017, **2**, 271–282.

3 S. Liu, J. Xiao, X. F. Lu, J. Wang, X. Wang and X. W. (David) Lou, *Angew. Chem., Int. Ed.*, 2019, **58**, 8499–8503.

4 J. Wang, T. Cheng, A. Q. Fenwick, T. N. Baroud, A. Rosas-Hernández, J. H. Ko, Q. Gan, W. A. Goddard and R. H. Grubbs, *J. Am. Chem. Soc.*, 2021, **143**, 2857–2865.